Bicoherence in electrostatic turbulence driven by high magnetohydrodynamic activity in Tokamak Chauffage Alfvén Brésilien

G. Z. dos Santos Lima, Z. O. Guimarães-Filho, A. M. Batista, I. L. Caldas, S. R. Lopes, R. L. Viana, I. C. Nascimento, and Yu. K. Kuznetsov

Articles you may be interested in

Electrostatic turbulence driven by high magnetohydrodynamic activity in Tokamak Chauffage Alfvén Brésilien
Phys. Plasmas **15**, 062501 (2008); 10.1063/1.2920211

Magnetohydrodynamic and turbulence activity analysis in the ISTTOK tokamak using empirical mode decomposition
Rev. Sci. Instrum. **77**, 10F512 (2006); 10.1063/1.2220474

Profile-turbulence interactions, magnetohydrodynamic relaxations, and transport in tokamaks
Phys. Plasmas **12**, 090907 (2005); 10.1063/1.2034387

Edge transport and the low-to-high transition in tokamaks with D-shaped magnetic flux surfaces
Phys. Plasmas **11**, 4280 (2004); 10.1063/1.1775010

Low to high confinement transition theory of finite-beta drift-wave driven shear flow and its comparison with data from DIII-D
Phys. Plasmas **11**, 1109 (2004); 10.1063/1.1638381

Bicoherence in electrostatic turbulence driven by high magnetohydrodynamic activity in Tokamak Chauffage Alfvén Brésilien

G. Z. dos Santos Lima,[1] Z. O. Guimarães-Filho,[1] A. M. Batista,[2] I. L. Caldas,[1]
S. R. Lopes,[3] R. L. Viana,[3,a]] I. C. Nascimento,[1] and Yu. K. Kuznetsov[1]

[1]*Instituto de Física, Universidade de São Paulo, Caixa Postal 66316, 05315-970 São Paulo, Brazil*
[2]*Departamento de Matemática e Estatística, Universidade Estadual de Ponta Grossa,
84032-900 Ponta Grossa, Paraná, Brazil*
[3]*Departamento de Física, Universidade Federal do Paraná, Caixa Postal 19044, 81531-990 Curitiba,
Paraná, Brazil*

During some discharges in Tokamak Chauffage Alfvén Brésilien [R. M. O. Galvão *et al.*, Plasma Phys. Controlled Fusion **43**, 1181 (2001)] high magnetohydrodynamic activity may appear with a peaked frequency spectrum. Whenever this peak occurs, the ambient broadband electrostatic turbulence is remarkably modified, synchronizing into the dominant magnetic fluctuation frequency and presenting high bicoherence in the whole plasma edge with a maximum bicoherence inside the plasma. A phenomenological model is introduced to investigate this driven turbulence bicoherence, consisting of nonlinearly coupled phase-randomized drift modes with time-periodic external driving at the dominant magnetic fluctuation frequency. The bicoherence spectrum of this model can mimic features of the experimental results. © *2009 American Institute of Physics*.
[DOI: 10.1063/1.3099701]

I. INTRODUCTION

In tokamaks, electrostatic turbulence is the main cause of the anomalous particle and energy transport at the plasma edge and its action is critical for the confinement performance.[1–3] Despite the recent theoretical[3–5] and experimental progress[6–8] on the understanding of this turbulence a complete description of the observations has not yet been achieved. Thus, further understanding is still necessary to complete the plasma edge description and to improve limiter and divertor designs for future tokamaks.

Electrostatic fluctuations have been usually described by their space and time behavior. Thus, the standard linear spectral analysis provides experimental information about the waves at the plasma edge and the particle transport driven by these waves.[9] However, to investigate the origin of the observed broadband fluctuation spectra and the instabilities or unstable waves that are delivering energy to the whole fluctuation spectrum it is necessary to identify the nonlinear wave-wave interaction. The bispectral analysis, a method to find three-wave coupling, allows one to discriminate between the coupled waves and those spontaneously excited by the plasma.[10–16]

With this method, in the Texas Experimental Tokamak, fluctuation data from Langmuir probes were used to identify three-wave interactions responsible for the redistribution of energy from the dominant unstable waves to other spectral components.[17,18] Since that early work, the bispectral analyzes have been applied to turbulence fluctuations of different toroidal devices. More recently, the bispectral analysis has been applied to study the time evolution of the spectral characteristics of intermittent bursts and the transition from *L* (low) to *H* (high) confinement mode,[19–22] precursors of edge localized modes,[23,24] and other transient events in fusion plasmas.

Moreover, bispectral analyzes were also used to identify the nonlinear coupling and structures in the onset of turbulence in magnetically confined plasmas different from those found in fusion devices.[25–27] However, even though in recent years the application of the bicoherence method to analyze plasma turbulence data has increased, the interpretation of bicoherence data still requires a detailed study.[28,29]

A number of experiments in tokamaks indicate that electrostatic turbulence can be driven by Mirnov oscillations. The first observation of this phenomenon has been made in Texas Experimental Tokamak Upgrade, where the turbulence level was enhanced for large magnetohydrodynamic (MHD) activity discharges with a 2/1 (where *m*=2 and *n*=1 are the poloidal and toroidal mode numbers, respectively) dominant mode with a measured frequency of 3 kHz. Moreover, the Mirnov oscillations have produced modulation of the edge density and floating potential.[30] This modulation has been also observed for other natural dominant magnetic modes in Brazilian Tokamak,[31] the Czech Academy of Sciences Torus[32,33] tokamaks, and in Tokamak Chauffage Alfvén Brésilien (TCABR), for a 2/1 dominant magnetic mode created by an ergodic magnetic limiter.[34]

During *L-H* transitions in the Joint Experiment Tokamak (JET) abrupt changes in the electric and magnetic fluctuation spectra have been observed.[35] Sudden changes in the spectra also appeared on the drift flow driven turbulence in the Large Plasma Device (LAPD).[36] The latter results can be explained by the generation of electromagnetic non-normal modes in drift-wave-zonal flow turbulence.[37,38]

In contrast with most tokamaks, in the TCABR the mag-

---

[a]]Author to whom correspondence should be addressed. Electronic mail: viana@fisica.ufpr.br.

netic and electrostatic frequency spectra present a peculiar partial superposition.[39] This may enhance the coupling, normally small, between these two kinds of fluctuations and opens the possibility of investigating this effect. Moreover, in some TCABR regimes the MHD activity increases at different instants of time during the discharge, and reaches high amplitudes with a narrow wave-number spectrum and a well-defined peak on the Mirnov frequency (~ 13 kHz).[40–42] During this high MHD activity the electrostatic turbulence synchronizes with the MHD activity at the Mirnov frequency and its broadband wave-number spectra is greatly modified.[42] This influence of the magnetic fluctuation on the electrostatic turbulence is observed only when the MHD activity amplitude is high enough and for some frequencies.

This kind of amplitude dependent synchronization on specific frequencies is commonly observed in other experimental nonlinear dynamical systems, as in chaotic electronic circuits perturbed by ac tensions.[43–45] Recently this kind of synchronization has also been observed in some plasma discharges in linear devices perturbed by time-periodic electric potentials.[46–48] Thus, the above mentioned observations in TCABR can be interpreted as an indication of an onset of nonlinear coupling between the magnetic and the electric fluctuations during periods of high MHD activity. Taken into account all these observations, it seems worthwhile to look for other evidences of such coupling in TCABR, as reported in this work.

The purpose of this article is twofold. Initially, we present further experimental evidence of electrostatic turbulence synchronization with the Mirnov frequency driven by magnetic fluctuations during high MHD activity in TCABR discharges. We employ bicoherence spectral analysis to quantify the intensity of the electrostatic turbulence synchronization as well as its radial dependence. We observe that the driven turbulence bispectrum is much modified by the high MHD activity and, consequently, presents the same regularity of this fluctuation with high bicoherence between the Mirnov frequency and the whole spectrum frequencies. In fact, this effect is most pronounced near the plasma edge position around the rational magnetic surfaces with the safety factor $q=3$. We conjecture that these bispectrum similarities appear due to a nonlinear coupling between the driving magnetic fluctuation and the electrostatic turbulence.

After presenting the experimental results, we interpret the observed modified turbulence state as being driven by the magnetic oscillation at a given dominant frequency. In such a case, the underlying dynamics would be similar to those creating limit cycles observed in other periodically driven nonlinear systems. Thus, similarly to other synchronized dynamical systems, while a nonlinear coupling modifies the turbulence, the observed spectra and bispectra only distinguish among states before and after the increase of the MHD activity. We consider this possibility and use a very simple theoretical model in order to try to mimic our experimental findings and obtain the observed final turbulence state, by considering a turbulent electric potential evolution with three modes nonlinearly coupled and driven by a time-periodic forcing representing the main magnetic fluctuation mode.

The rest of the paper is organized as follows: In Sec. II

we describe the experimental setting. Section III treats the bicoherence analysis of the turbulent spectrum we obtained from the TCABR with and without high MHD activity. Section IV presents a theoretical model we use to simulate the features observed in experiments, namely, the high bicoherence levels of electrostatic fluctuations driven by high MHD activity. Section V brings the bicoherence analysis of time series obtained from numerical simulations of this theoretical model. Section VI contains our conclusions.

II. EXPERIMENT

The experiments have been performed in the hydrogen circular plasma of the TCABR tokamak (major radius $R=61$ cm and minor radius $a=18$ cm).[40] The plasma current reaches a maximum value of 100 kA, with duration 100 ms, the hydrogen filling pressure is 3×10^{-4} Pa, and toroidal magnetic field $B_0=1.1$ T. At the plasma edge the electron plasma density is $n_e \approx 3 \times 10^{18}$ m^{-3}, and the electron temperature is $T_e \approx 10$ eV.

The floating electrostatic potential has been measured in the region comprising the plasma edge and the scrape-off layer ($0.9 < r/a < 1.2$) by a set of three movable electrostatic probes. Two of them were placed in two poloidal positions separated by 0.4 cm, yielding the floating potentials, φ_1 and φ_2, at the corresponding positions. The third probe, used to measure the ion saturation current I_S, was placed at a toroidal position 0.4 cm apart from the poloidal probes. The whole set was mounted at the inner equatorial region of the tokamak. Magnetic fluctuations were detected using a Mirnov coil located at $r=19.5$ cm (i.e., 1.5 cm outside the plasma radius). Radial profiles of electrostatic fluctuations were obtained on shot-to-shot basis. Probe and Mirnov coil data were digitized at 1 and 0.25 Msample/s, respectively, and filtered by a 300 kHz antialiasing filter.

Figure 1 shows the time evolution of a typical plasma discharge in TCABR. The plasma current [Fig. 1(a)] grows rapidly in the first milliseconds until ~ 50 kA, then increases at a slower rate until reaching a short plateau where the current stays at a 100 kA level, decaying slowly during the second half of the discharge. The central chord-integrated electron density, indicated by Fig. 1(b), exhibits a similar evolution, with a first plateau level of $n_e \sim 1.0 \times 10^{19}$ m^{-3}, which roughly coincides with the slower current ramp, and is followed by a second plateau of $\sim 1.2 \times 10^{19}$ m^{-3} between 40 and 60 ms. During the rest of the discharge the density decreases gently until disruption. It is interesting to observe that during this second (and higher) plateau of the plasma density the magnetic activity is high.

The MHD activity measured by the coils, or the fluctuations of the poloidal field time rate, $\dot{\tilde{B}}$, are depicted in Fig. 1(c). These oscillations are spontaneously produced in the plasma and can be observed quite often during the first milliseconds of the discharge, although a major burst of magnetic activity can be clearly observed after ~ 40 ms, with a duration of about 20 ms. After this event the magnetic activity is reduced to a noisy level.

A glimpse of the coupling effect between magnetic and electrostatic oscillations we are to describe can be already
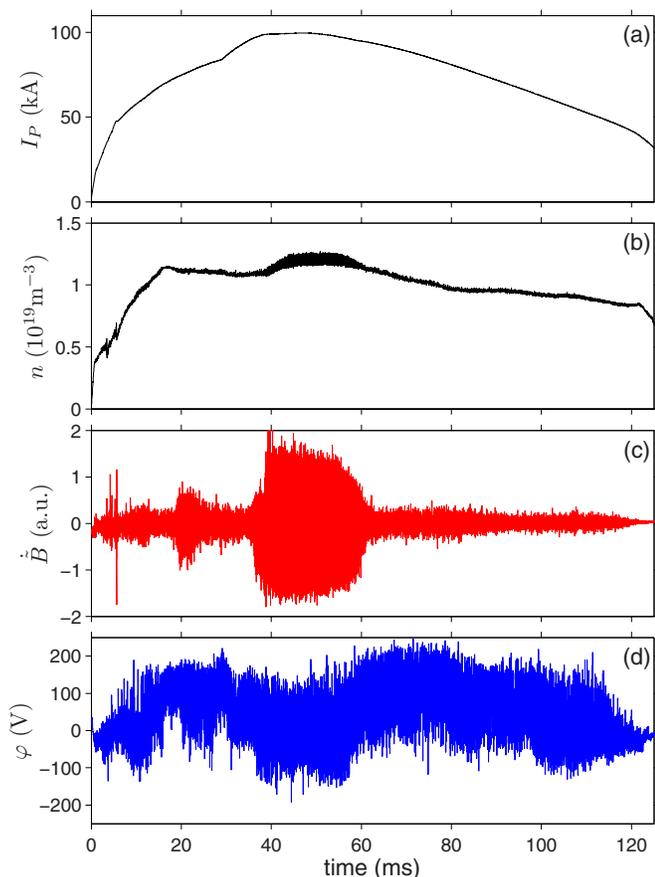
FIG. 1. (Color online) Time evolution of the (a) plasma current, (b) central chord-integrated plasma density, (c) MHD activity, and (d) floating potential (at $r_S/a = 0.97$) for a discharge of TCABR.

FIG. 2. (Color online) Fourier power spectral density (arbitrary units) for (a) Mirnov oscillations and (b) electrostatic potential at $r_S/a = 0.97$ during the discharge of Fig. 1. Fluctuating electrostatic potential (c) before and (d) during the period with high MHD activity.

observed in Fig. 1(d), where the time evolution of the floating electrostatic potential φ_1 is depicted along the discharge. During the burst of magnetic activity started at 40 ms, the electrostatic fluctuations are strongly affected. Moreover, after the magnetic burst ceases, the electrostatic fluctuations resume to their former behavior.

This is obviously a purely factual evidence and needs to be quantified by using appropriate measures, like the Fourier spectra of both magnetic and electrostatic fluctuations, the results being depicted in Fig. 2 for magnetic and electrostatic measurements, the latter performed at a fixed radius $r = 17,5$ cm. In the spectrograms, the oscillation frequencies (in kilohertz) are plotted against the discharge duration, the corresponding power spectral densities (in arbitrary units) being plotted in a color scale. Figure 2(a) exhibits the spectrogram for Mirnov oscillations, where the periods of magnetic activity are associated with peaks of the power spectral density S_{BB}. In particular, the intense burst started at 40 ms has a sharp line with a dominant frequency of ~13 kHz which extends up to 60 ms, with at least two overtones corresponding to higher harmonics of the dominant frequency. The occurrence of high MHD activity coincides with the synchronization of the electrostatic potential fluctuations [Fig. 2(b)]. The characteristic broadband spectrum of turbulent fluctuations, after the episodes of magnetic activity, is punctured with peaks (or lines for running time) at the same

frequencies of the magnetic fluctuations. Representative examples of the time series for the electrostatic oscillations without and with high magnetic activity are given in Figs. 2(c) and 2(d), respectively.

III. BICOHERENCE ANALYSIS OF EXPERIMENTAL DATA

The MHD oscillations drive the electrostatic fluctuations in the sense that both present similar spectral peaks, which is in fact an example of synchronization of turbulent signals, that we have previously studied using Fourier and wavelet analysis.[42] For a broadband turbulence spectrum, the bispectral analysis is the standard procedure to detect and quantify the amount of mode coupling in a given signal. Mode coupling, on its way, must result from nonlinear interactions which may be thought of as quadratic, in a first approximation.

As a result from such nonlinear interaction, two modes with frequencies f_1 and f_2 can interact to generate a third mode with frequency f_3, which is phase coupled to the other two modes. In this quadratic three-mode nonlinear process the mode frequencies must obey the resonance condition $f_1 + f_2 = f_3$. However, for regular oscillations, the phase differences between three modes can remain constant giving a high value of bicoherence without any nonlinear coupling if their frequencies obey the resonant condition.

The power spectrum is the Fourier transform of the autocorrelation (or second-order cumulant) function, and it is well suited to deal with linear processes. For broadband spectra, nonlinear mode couplings that occur in triads, as described above (for quadratic nonlinearities) demand the
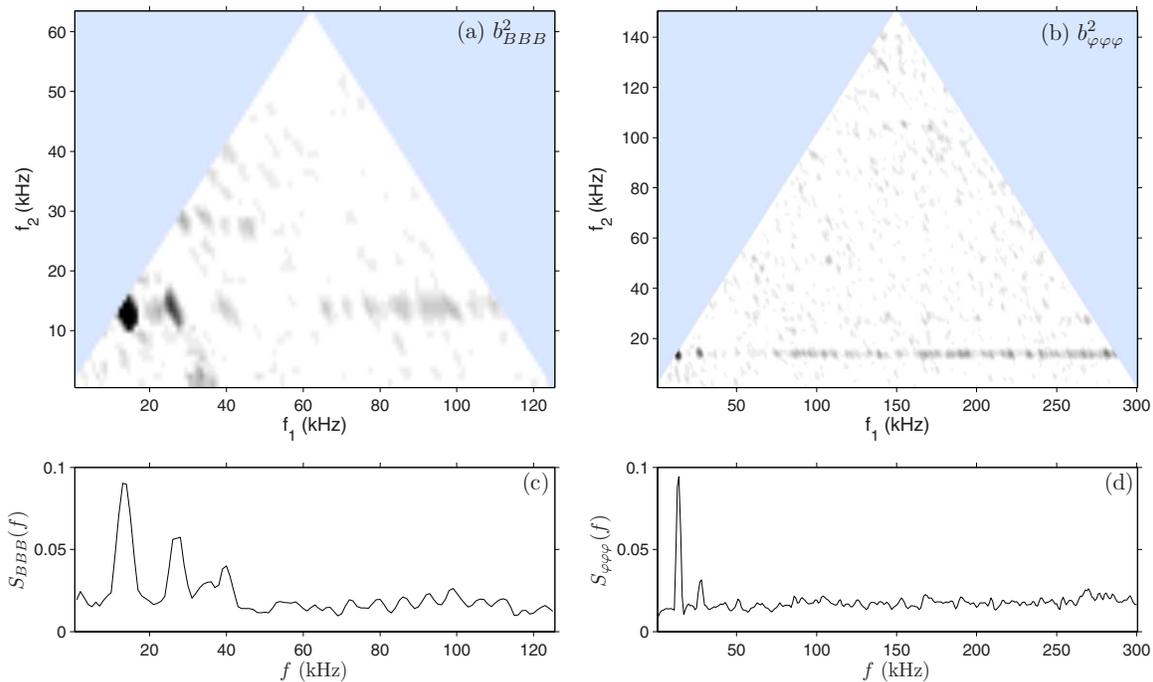
FIG. 3. (Color online) Bicoherence spectrum of (a) magnetic (b_{BBB}^2) and (b) electrostatic ($b_{\varphi\varphi\varphi}^2$) oscillations during high MHD activity (between 40 and 60 ms). (c) and (d) are plots of the summed bicoherence corresponding to (a) and (b), respectively.

use of higher-order statistics. The bispectrum is the Fourier transform of the third-order cumulant-generating function. Let $\phi(f)$ be the Fourier transform of the time signal at the mode frequency f. The bispectrum is defined as[12]

$$\mathcal{B}(f_1, f_2) = \langle \phi(f_1)\phi(f_2)\phi^*(f_3) \rangle, \qquad (1)$$

which can be further normalized by introducing the associated bicoherence

$$b^2(f_1, f_2) = \frac{|\mathcal{B}(f_1, f_2)|^2}{\langle |\phi(f_1)\phi(f_2)|^2 \rangle \langle |\phi(f_3)|^2 \rangle}, \qquad (2)$$

such that $0 \leq b^2 \leq 1$ and, accordingly, and can be used as a measure of the amount of nonlinear coupling between the modes in the triplet with frequencies f_1, f_2, and f_3. If the three modes are phase coupled, there follows that b^2 is near the unity; whereas it is almost zero if the modes are barely or no coupled at all. The summed bicoherence $S(f) = \Sigma b^2(f_1, f_2)$ measures the amount of coupling at the frequency f relative to all other frequencies, i.e., we sum over all frequency satisfying the resonance condition $f = f_1 + f_2$.

Since we are quantifying the intensity of bicoherence in both electrostatic and magnetic time series, we shall distinguish them by using the following notations for the bicoherence: $b_{\varphi\varphi\varphi}^2$ and b_{BBB}^2, respectively, with a corresponding notation for the summed bicoherence. We present the bicoherence spectrum (in a gray scale for which darker shades of gray indicate larger values of b^2) as a function of the two frequencies f_1 and f_2 for magnetic and electrostatic signals in Figs. 3(a) and 3(b), respectively. We have chosen the time window (between 40 and 60 ms) corresponding to the occurrence of the major burst of spontaneous MHD activity [cf. Fig. 1(c)] in order to evidence the coupling between magnetic and electrostatic modes.

The most pronounced peak of bicoherence in magnetic oscillations is centered at $f_1 = f_2 \approx 13$ kHz, indicating a strong coupling between these frequencies and a third mode with $f_3 \approx 26$ kHz. Coupling can also be detected in this way along a rough line of $f_1 \approx 13$ kHz. The second peak, centered at $f_1 \approx 26$ kHz, resonates with a third mode $f_3 \approx 39$ kHz and so on. While the first peaks of bicoherence correspond to the peak at ≈ 13 kHz in the spectrogram of Fig. 2(a), the other ones have probably nonlinear origin and can be properly resolved only by the bispectrum. Moreover, these peaks carry most of the bispectral content, as shown in the summed bicoherence plotted in Fig. 3(c).

A similar picture is displayed in the bicoherence spectrum of electrostatic oscillations [Fig. 3(b)] as well as in the summed bicoherence [Fig. 3(d)]. There is a line of high bicoherence along $f_1 \approx 13$ kHz, with peaks roughly at the same values as in the magnetic bicoherence. It is important to note that the presence of peaks in the bicoherence spectra only indicates that there are modes whose phase differences remain nearly constant. In the present case, these peaks are related with an unusual regular variation of the electrostatic oscillations at the MHD frequencies due to the coupling involving the magnetic and electrostatic fluctuations. So, the bicoherence of electrostatic signals in this work is used to label the strength of the MHD influence over the electrostatic turbulence.

In order to investigate the radial dependence of the electrostatic turbulence synchronization we plot in Figs. 4(b) and 4(c), respectively, radial profiles of the maximum values of the bicoherence for floating potential (blue points) and ion saturation current (black points). These points correspond, in both figures, to episodes of strong magnetic activity. The Mirnov coils that measure magnetic oscillations are fixed at a
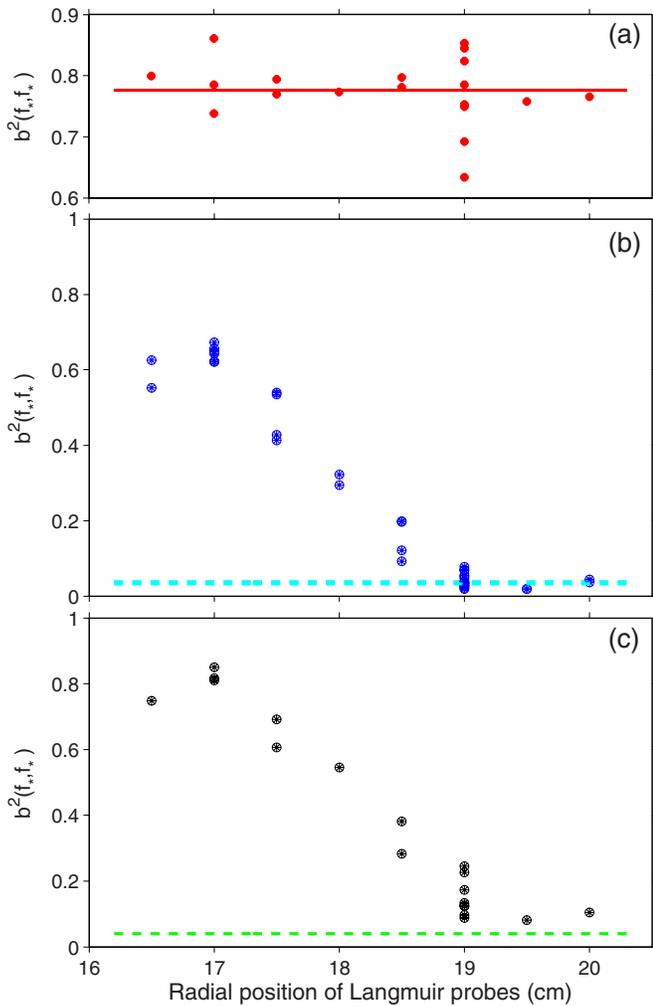
FIG. 4. (Color online) (a) The bicoherence of magnetic oscillations does not vary with the radius, but their values are represented as red points, and their mean by a red line. Radial profiles of the maximum bicoherence spectra of signals of (b) floating potential (blue points) and (c) ion saturation current (black points), during periods of strong MHD activity. The blue and green dashed lines in (b) and (c), respectively, indicate the corresponding values for periods of weak or no MHD activity.

radial position ($r = 19.5$ cm) and thus the red points in Fig. 4(a) represent different results with no radial dependence. They have been put in the same graphs only for comparison of the reproducibility of the considered discharges with respect to the values of the bicoherences observed in the magnetic signals.

According to Fig. 4(b) the electrostatic bicoherence increases as we approach a maximum radius of 17 cm, 1 cm before the plasma column radius, and decreases afterwards to a minimum value at the scrape-off layer. The behavior is essentially the same for the ion saturation current measurements [Fig. 4(c)]. It is remarkable that this radial dependence holds only during the strong MHD activity since the corresponding values of the maximum bicoherence without magnetic activity are very low [they have been indicated by blue and red lines in Figs. 4(b) and 4(c), respectively]. This turbulence bicoherence enhancement and its radial dependence may be regarded as an indication of coupling between the electrostatic and the magnetic oscillations. The radial posi-

tion of these maxima agrees with the position where the higher value of the synchronization intensity was observed in TCABR (Ref. 42) and corresponds to the 3/1 resonant magnetic surface position.

We conjecture that a nonlinear coupling modifies the turbulence bicoherence until the latter assumes the observed similarity with the magnetic bicoherence. Thus, we may be observing the turbulence final state and not the turbulence transition driven by high MHD activity. Other interpretations could also be considered to explain the observed spectrum and bispectrum similarities. For instance, an interaction between a saturated nonlinear tearing mode and the turbulence, which modifies the equilibrium so as to yield large magnetic islands.[39] Another possibility could be the onset of a non-modal linear instability, for which the similarities between the observed spectra reveal a global mode consisting on both magnetic and electric fluctuations.[38,39]

IV. A PHENOMENOLOGICAL MODEL OF ELECTROSTATIC OSCILLATIONS

In this section we develop a phenomenological model based on the conjecture that the observed synchronization and bicoherence could be interpreted as an evidence of nonlinear coupling between the magnetic and electric fluctuations, such as observed in linear plasma devices.[46–48]

The bicoherence spectrum of the electrostatic turbulence shows oscillations satisfying the triplet resonance condition $f_1 + f_2 = f_3$. Since these oscillations have also a broadband frequency spectrum (with too small bicoherence levels to be resolved by bispectral analysis), they can be modeled as being chaotic, if their deterministic content is high enough to point significant deviations from purely random fluctuations. A previous analysis of recurrences in turbulent fluctuations in the plasma edge of TCABR has indicated a pronounced deterministic content of the floating potential oscillations, in addition to a random component.[49]

Hence it is quite natural to look for deterministic models of three waves with quadratic interactions to describe the deterministic content of electrostatic potential fluctuations. One such model is based on a three-mode truncation of the Hasegawa–Mima equation describing low-frequency drift waves.[50] It is also necessary to add phenomenological growth/decay rates for the triplet waves in order to include the energy injection in the triplet and its redistribution among the different interacting modes.[51]

We start from the so-called Hasegawa–Mima equation, which governs the spatiotemporal evolution of the electrostatic potential $\phi(\mathbf{x}, t)$ of a drift-wave

$$\frac{\partial}{\partial t}(\nabla^2 \phi - \phi) - [(\nabla \phi \times \hat{\mathbf{z}}) \cdot \nabla]\left[\nabla^2 \phi - \ln\left(\frac{n_0}{\omega_{ci}}\right)\right] = 0, \quad (3)$$

where n_0 is the background plasma density, $\omega_{ci} = eB_0/m_i$ is the ion-cyclotron frequency, $\mathbf{B}_0 = B_0\hat{\mathbf{z}}$ is the toroidal magnetic field, and e and m_i are the ion charge and mass, respectively. The operator ∇ stands for the gradient with respect to directions transverse to the magnetic field: $\nabla = \hat{\mathbf{x}} \partial/\partial x + \hat{\mathbf{y}} \partial/\partial y$. The rectangular geometry we use in our treatment is a large aspect-ratio approximation for the tokamak plasma edge, for

which curvature effects are negligible in both toroidal and poloidal directions. In this case, the coordinates (x, y, z) stand for the radial position measured from the tokamak wall, the rectified poloidal and toroidal angles, respectively.

In the derivation of Eq. (3) it is assumed that the drift-wave frequency ω is much smaller than ω_{ci}, where the phase velocity along the magnetic field is such that $v_{T_i} < (\omega/k_z) < v_{T_e}$, where v_{T_s} is the thermal velocity for ions $(s = i)$ and electrons $(s = e)$, and (k_x, k_y, k_z) are the wave vector components. The drift-wave dispersion relation is[52]

$$\omega = \omega_{\mathbf{k}} = -\frac{1}{1 + k^2}\left[(\mathbf{k} \times \hat{\mathbf{z}}) \cdot \nabla \ln\left(\frac{n_0}{\omega_{ci}}\right)\right]. \qquad (4)$$

Drift waves have a characteristic dispersion scale length $\rho_s = \sqrt{T_e/m_i\omega_{ci}^2}$, where T_e is the electron temperature, and which turns to be the fundamental electric cross-field shielding distance for charge clumps in the regime of drift-wave fluctuations. In Eq. (3) the coordinates x, y, z have been rescaled by ρ_s, the time by ω_{ci}, and the potential by T_e/e.

A Fourier mode expansion of the electrostatic potential reads

$$\phi(\mathbf{x}, t) = \frac{1}{2}\sum_{j=1}^{\infty}\left[\phi_{\mathbf{k}_j}(t)\exp(i\mathbf{k}_j \cdot \mathbf{x}) + \phi_{\mathbf{k}_j}^*(t)\exp(-i\mathbf{k}_j \cdot \mathbf{x})\right], \qquad (5)$$

where $\phi_{\mathbf{k}_j}(t)$ is a complex mode amplitude at a fixed position $\mathbf{x}$, corresponding to a wave vector $\mathbf{k}_j$, and the asterisk stands for the complex conjugate. Substituting Eq. (5) into Eq. (3) yields an infinite system of coupled differential equations for the mode amplitudes[53]

$$\frac{d\phi_{\mathbf{k}_j}}{dt} + i\omega_{\mathbf{k}_j}\phi_{\mathbf{k}_j} = \sum_{(\mathbf{k}_\alpha, \mathbf{k}_\beta, \mathbf{k}_\gamma)}\Lambda_{\mathbf{k}_\beta, \mathbf{k}_\gamma}^{\mathbf{k}_\alpha}\phi_{\mathbf{k}_\beta}^*\phi_{\mathbf{k}_\gamma}^*, \qquad (6)$$

where $j = 1, 2, 3, \ldots$, and the summation runs over those wave vector triplets which satisfy the resonant condition $\mathbf{k}_\alpha + \mathbf{k}_\beta + \mathbf{k}_\gamma = \mathbf{0}$ for any choice of $\mathbf{k}_j$. The drift-wave mode frequencies are given by the dispersion relation (4), and the coupling coefficients are given by

$$\Lambda_{\mathbf{k}_\beta, \mathbf{k}_\gamma}^{\mathbf{k}_\alpha} = \frac{(\mathbf{k}_\gamma^2 - \mathbf{k}_\beta^2)}{2(1 + \mathbf{k}_\alpha^2)}(\mathbf{k}_\beta \times \mathbf{k}_\gamma) \cdot \hat{\mathbf{z}}. \qquad (7)$$

We make a three-mode truncation of the coupled system of equations in Eq. (6) such that the resonance conditions are satisfied,

$$\mathbf{k}_1 + \mathbf{k}_2 + \mathbf{k}_3 = \mathbf{0}, \qquad (8)$$

$$\omega_{\mathbf{k}_1} + \omega_{\mathbf{k}_2} + \omega_{\mathbf{k}_3} \approx 0. \qquad (9)$$

Note that the second condition holds only in an approximate way, i.e., we allow for a (small) frequency mismatch. The three-mode system reads[53]

$$\frac{d\phi_1}{dt} + i\omega_1\phi_1 = \Lambda_{2,3}^1\phi_2^*\phi_3^* + \gamma_1\phi_1, \qquad (10)$$

$$\frac{d\phi_2}{dt} + i\omega_2\phi_2 = \Lambda_{3,1}^2\phi_3^*\phi_1^* + \gamma_2\phi_2, \qquad (11)$$

$$\frac{d\phi_3}{dt} + i\omega_3\phi_3 = \Lambda_{1,2}^3\phi_1^*\phi_2^* + \gamma_3\phi_3, \qquad (12)$$

where we use the shorthand notation: $\phi_j = \phi_{\mathbf{k}_j}$ and $\omega_j = \omega_{\mathbf{k}_j}$. We have introduced phenomenological terms in the coupled mode equations to represent the energy injection/dissipation necessary to sustain the wave interactions, such that γ_i are growth/decay coefficients.

The bicoherence similarities presented in Sec. III suggest that there is coupling between electrostatic and magnetic oscillations due to a cause-effect relationship still unknown. The Mirnov oscillations are fluctuations of the poloidal field $\widetilde{B}$ that combine with the equilibrium magnetic field so as to modify the $(\mathbf{E} \times \mathbf{B})$-drift velocity. The drift changes in charged particle orbits are likely to modify the floating potential fluctuations as well. However, a fundamental physical description of this coupling should be investigated by using basic equations describing coupled magnetic and electrostatic oscillations as, for example, the reduced resistive MHD equations.[54]

On the other hand, in the spirit of this section we mimic the effect of this coupling by a source term added to the three-mode Eqs. (10)–(12). Let us represent its effect by a time-periodic driving term $\exp(\pm i\Omega t)$, where Ω is the dominant Mirnov oscillations frequency. The kind of coupling that furnished the best results was obtained by adding a source term $B\cos^2(2\pi\Omega t)$ to all three modes, where B is a parameter that measures the coupling strength between magnetic and electrostatic oscillations. Its value, as well as other parameters to be introduced below, is chosen as to match the bicoherence results observed in the experiments.

The dynamics generated by the driven three-mode equations is still purely deterministic, and we can find wide parameter ranges (even in the unforced case[55]) for which the three-mode system described by the above equations displays chaos in the phase space whose dimensions are given by the Fourier mode amplitudes. This regime persists also in the phase space formed by the real electrostatic potential modes.[55] We mean chaotic dynamics in the sense that the phase trajectories $[\phi_1(t), \phi_2(t), \phi_3(t)]$ stemming from initial conditions $[\phi_1(0), \phi_2(0), \phi_3(0)]$ have positive maximal Lyapunov exponent.[56] One of the characteristic features of chaotic orbits is that they present recurrences, i.e., given some actual state $[\phi_1(t_1), \phi_2(t_1), \phi_3(t_1)]$, one comes back to some neighborhood of it after a given time interval $t_2 > t_1$. This means that there is some small neighborhood radius ϵ for which the distance (in phase space) between the orbit points at t_1 and t_2 is less than ϵ. For strongly chaotic systems the value of ϵ can be arbitrarily small, i.e., the orbits will always recur, no matter how long does it take.[57]

A quantitative analysis of the recurrence level present at some time series, such as the floating electrostatic potential measured by the Langmuir probe at a fixed radius, is the recurrence quantification analysis (RQA).[58] The use of RQA is promising in tokamak measurements, since data from tur-

bulent plasmas are expected to be have both deterministic and stochastic features. One of the advantages of RQA is that it is capable to distinguish deterministic chaos from random fluctuations and, to some extent, to quantify their relative contribution to some signal. For example, one of the tools provided by RQA, the so-called determinism, measures our ability to detect the amount of determinism in a given time series. Recent results of RQA have shown that floating potential signals in TCABR have a significant deterministic content, especially at the plasma edge.[49]

The recurrence-based analysis of results suggested the use of three quadratically coupled wave, whose governing equations were endowed with an additive noise term in order to mimic the stochastic content present in the electrostatic oscillations measured in TCABR. Since one of the roles of extrinsic noise is to randomize phases, we have introduced noise in the three-mode Eqs. (10)–(12) in the following way: we integrated numerically Eqs. (10)–(12) using a fourth-order Runge–Kutta scheme with fixed step size Δt. This step size is taken as a fraction of the cyclotronic frequency used in the normalization of time in the differential Eqs. (10)–(12). At each integration step we computed the phase $\theta_j(t) = \arctan[b_j(t)/a_j(t)]$ associated with the Fourier mode amplitude $\phi_j(t) = a_j(t) + ib_j(t)$, $j = 1, 2, 3$, and add a noiselike term Ar_t to the value obtained, where A is the noise level, and r_t is a pseudorandom variable chosen from a Gaussian probability distribution with zero mean and unit variance. After this addition we reconstruct the value of $\phi_j(t) = |\phi_j(t)| \exp[i(\theta_j(t) + Ar_t)]$ and resume integration. It is because of this procedure that we cannot use a predictor corrector or even a simpler variable step size integration scheme: Since the variable values change in a random fashion at each integration step, we cannot go backward and compare present and past values for refining the integration interval.

V. BICOHERENCE ANALYSIS OF NUMERICAL SIMULATIONS

In the numerical simulations using Eqs. (10)–(12) with driving and noise, we used parameter values compatible with the tokamak TCABR. The electron temperature was taken to be $T_e = 10$ eV; and the density gradient is $|\nabla n_0|/n_o = 5$ m^{-1}, from which we estimated the ion-cyclotron frequency to be 1.05×10^8 Hz and the length scale is thus $\rho_s \approx 10^{-3}$ m. The radial density gradient at the plasma edge was estimated, on the basis of particle flux measurements, to be[59]

$$\mathcal{N} := \rho_s \left| \nabla \ln\left(\frac{n_0}{\omega_{ci}}\right) \right| = \rho_s \left| \frac{\nabla n_0}{n_0} \right| \approx 1.0 \times 10^{-3}. \quad (13)$$

Fourier and wavelet spectral analyses of electrostatic potential fluctuations, in discharges where the MHD activity is not too high, give a poloidal wave number k_y in the range of $(1-5) \times 10^3$ m^{-1}, with a broad spectral content in the kilohertz range, and concentrated at frequencies below 50 kHz;[60] the latter being in accordance with the results shown in Sec. II. The other wave vector components were estimated using linear relations and applying the resonance condition of three-mode coupling. The normalized frequencies were cho-

sen as $\omega_1 = 6.6 \times 10^{-4}$, $\omega_2 = 4.2 \times 10^{-4}$, and $\omega_3 = 2.4 \times 10^{-4}$, related to the wave vector components by the dispersion relations[55]

$$\omega_i = \frac{(k_{iy} - k_{ix})}{1 + k_i^2} \mathcal{N}, \quad (i = 1, 2, 3), \quad (14)$$

from which we can estimate the coupling coefficients in Eqs. (10)–(12) as $\Lambda_{2,3}^1 = -1.15 \times 10^{-2}$, $\Lambda_{3,1}^2 = 5.30 \times 10^{-3}$, and $\Lambda_{1,2}^3 = 6.00 \times 10^{-4}$. Moreover, the time-periodic driving term representing the influence of magnetic oscillations has a normalized frequency $\Omega = 9.0 \times 10^{-4}$.

We assume that ϕ_1 is the inductor wave, which pumps energy to the daughter waves ϕ_2 and ϕ_3; and the values of their growth/decay coefficients are adjusted to the measured range for the floating electrostatic potential:[60] $\gamma_2 = \gamma_3 = -35 \times 10^{-4}$ and $\gamma_1 = 3.0 \times 10^{-4}$. The remaining parameters used in the simulations are the noise level A and the strength of electric-magnetic coupling B, and which have been chosen to fit both the spectrogram and the bicoherence results from experimental data presented in Sec. III.

We recall that $\phi_{1,2,3}$ are (complex) mode amplitudes in the Fourier phase space. In order to compare the results of numerical simulations with experiments we have to reconstruct first the signal in the real phase space. Thus we fix the spatial position by taking a point near the tokamak wall, located at $x = y = 0$, and consider the time series of the predicted electrostatic signal given by the sum of the real parts of the three-mode Fourier mode amplitudes as in Eq. (5),

$$\phi(0, t) = \tfrac{1}{2}[\phi_1(t) + \phi_2(t) + \phi_3(t) + \text{c.c.}], \quad (15)$$

which can be dimensionalized, whenever necessary, by multiplying by the factor T_e/e.

In Figs. 5(a) and 5(b) we exhibit the normalized time series and the related spectrogram, respectively, for the signal $\phi(0, t)$ without both noise and driving ($A = B = 0$), and which may be accordingly called *coherent* three-mode equations. The time evolution of the mode amplitude, although clearly irregular (actually chaotic) [Fig. 5(a)], presents various frequency peaks [Fig. 5(b)], which is not compatible with the experimental spectrogram depicted in Fig. 2(b). Adding the stochastic term to the phase of this mode, with noise level $A = 0.35$, to the unforced three-wave equations, gives a turbulent electrostatic signal [Fig. 5(c)] with a clear broadband content [Fig. 5(d)].

A representative example of a signal mimicking the effect of coupling between electrostatic and Mirnov oscillations is depicted in Fig. 5(e), where the main peak of the respective spectrogram [Fig. 5(f)] coincides with the dominant Mirnov frequency that represents the MHD activity effect. The overtones that are also visible in the spectrogram, just like in the experimental case [Fig. 2(b)], result from the nonlinear resonance of the chaotic oscillation with the time-periodic forcing, which excites harmonics of the driving frequency.

The bicoherence spectrum for the incoherent (i.e., noisy) but unforced time series from numerical simulation is displayed by Fig. 6(a). The broadband Fourier spectrum already seen in Fig. 5(d) exhibits only low-amplitude fluctuations,
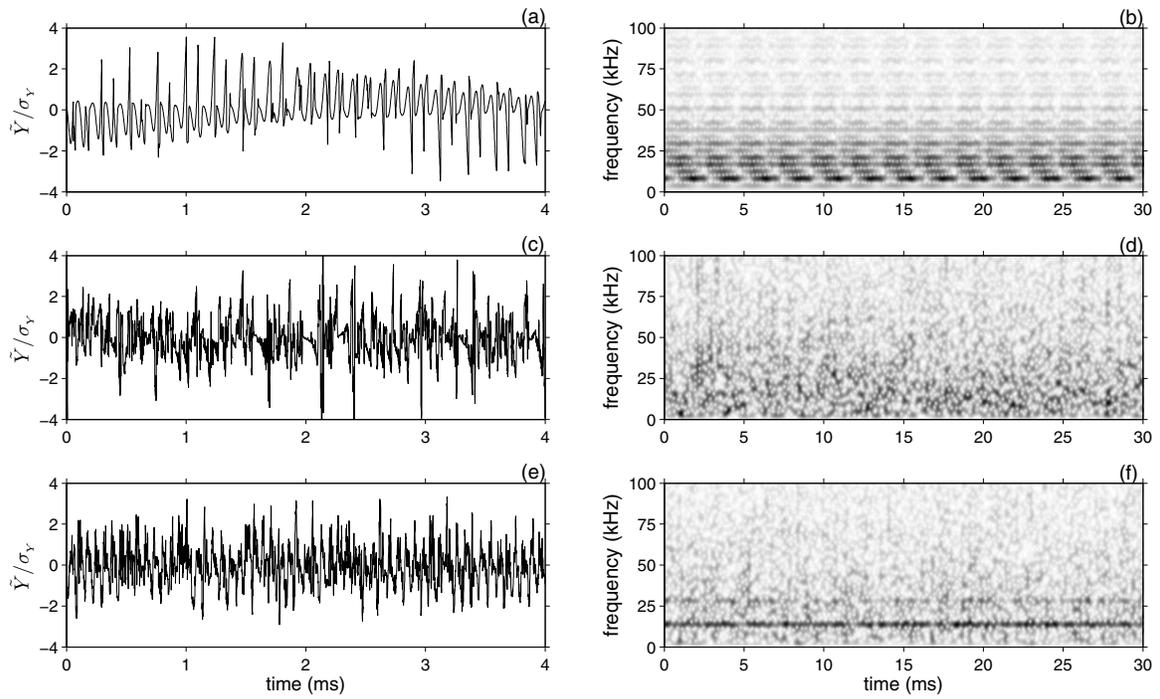
FIG. 5. Time evolution of the normalized electrostatic oscillation amplitude obtained from numerical integration of Eqs. (10)–(12) with (a) $A=B=0$; (c) $A=0.35$, $B=0$; (e) $A=0.35$, $B=0.03$. The spectrograms in (b), (d), and (f) correspond to (a), (c) and (e), respectively.

regarded as a natural consequence of the statistical fluctuations due to the finite length of the time series used in the bispectrum analysis. One must note that the added noise has destroyed some of the bicoherence, since the phases at different times have been randomized, what has immediate consequences in the frequency bicoherence spectrum. In fact, the summed bicoherence [Fig. 5(c)] does not show clearly dis-

tinguishable peaks, reinforcing the nonexistence of a systematic preference in the distribution of coupled modes that spread over a wide frequency range. We did not observe a significant mode coupling effect in the data from discharges without strong MHD activity.

High bicoherence is clearly seen, though, in Fig. 6(b), where both noise and driving are added to the chaotic three-
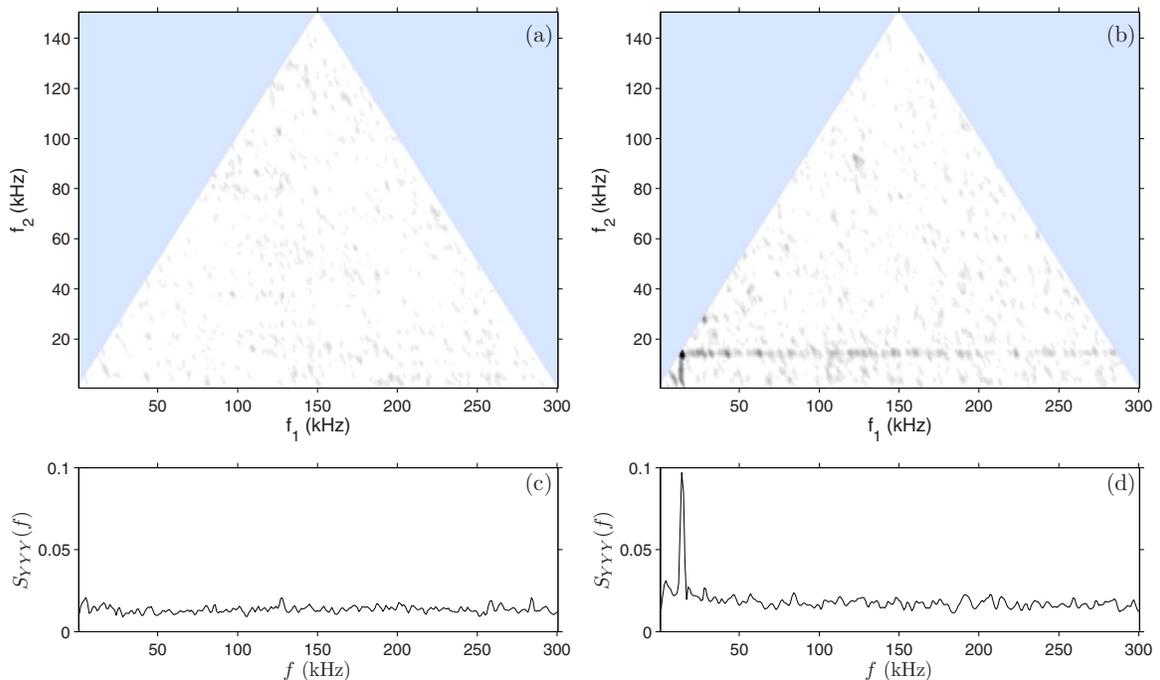
FIG. 6. (Color online) Bicoherence spectrum of electrostatic oscillations ($b^2_{\phi_t\phi_t\phi_t}$) obtained from numerical integration of Eqs. (10)–(12) with (a) $A=0.35$, $B=0$; (b) $A=0.35$, $B=0.03$. (c) and (d) are plots of the summed bicoherence corresponding to (a) and (b), respectively.

mode evolution. We can distinguish the same line of peaks, at the characteristic frequency of the driving term, that appears in the bicoherence of experimental data. Moreover, the distribution of these peaks along the frequency range is quite concentrated at this driving frequency, as confirmed by the corresponding summed bicoherence [Fig. 6(d)].

VI. CONCLUSIONS

Previous works have shown that during TCABR tokamak discharges with high MHD activity, the electrostatic plasma edge turbulence and the turbulence driven particle transport are strongly influenced by this activity at its dominant frequency.[33,40,41] Furthermore, a synchronization between the electrostatic turbulence and the MHD activity, at the same dominant frequency, has been observed in these discharges.[42]

In this paper, where we also considered TCABR discharges with high MHD activity, we reported other common characteristics between the electrostatic plasma edge turbulence and the high MHD activity. We identified similar bicoherence spectra involving the MHD frequency, for each of these fluctuations, by applying bicoherence analysis to the results of measurements in TCABR using a Langmuir probe and Mirnov coil for electrostatic and magnetic oscillations, respectively. For the electrostatic turbulence it was possible to obtain the radial profile of the coupling strength, with a local maximum at the 3/1 resonant magnetic flux surface position. Moreover, it should be noticed that none of the reported characteristics have been observed in TCABR discharges without high MHD activity.

As a complement of the foregoing data analysis, we simulated numerically the coupling between electrostatic and magnetic fluctuations using a chaotic dynamical system based on three coherent nonlinearly coupled drift modes with incoherent noise and a time-periodic driving at the MHD frequency. The addition of incoherent noise was used to reproduce both the linear and nonlinear spectral characteristics of turbulence data without high MHD activity. The external time-periodic driving term was introduced to reproduce spectral features observed during high MHD activity. An improved model for explaining the effect of the MHD activity on electrostatic oscillation would require a first-principles approach based on fluid and/or kinetic equations describing the coupling of the magnetic and electrostatic oscillations under the conditions of the analyzed experiments. These investigations should consider the influence of chaotic magnetic fields on the tokamak turbulence as well.[37,38,61]

ACKNOWLEDGMENTS

[1] A. H. Boozer, Rev. Mod. Phys. **76**, 1071 (2005).
[2] Ch. P. Ritz, R. V. Bravenec, P. M. Schoch, R. D. Bengtson, J. A. Boedo, J. C. Forster, K. W. Gentle, Y. He, R. L. Hickok, Y. J. Kim, H. Lin, P. E. Phillips, T. L. Rhodes, W. L. Rowan, P. M. Valanju, and A. J. Wootton, Phys. Rev. Lett. **62**, 1844 (1989).
[3] W. Horton, Rev. Mod. Phys. **71**, 735 (1999).
[4] C. Hidalgo, C. Alejaldre, A. Alonso, J. Alonso, L. Almoguera, F. de Aragón, E. Ascasíbar, A. Baciero, R. Balbín, E. Blanco, J. Botija, B. Brañas, E. Calderón, A. Cappa, J. A. Carmona, R. Carrasco, F. Castejón, J. R. Cepero, A. A. Chmyga, J. Doncel, N. B. Dreval, S. Eguilior, L. Eliseev, T. Estrada, J. A. Ferreira, A. Fernández, J. M. Fontdecaba, C. Fuentes, A. García, I. García-Cortés, B. Gonçalves, J. Guasp, J. Herranz, A. Hidalgo, R. Jiménez, J. A. Jiménez, D. Jiménez-Rey, I. Kirpitchev, S. M. Khrebtov, A. D. Komarov, A. S. Kozachok, L. Krupnik, F. Lapayese, M. Liniers, D. López-Bruna, A. López-Fraguas, J. López-Rázola, A. López-Sánchez, E. de la Luna, G. Marcon, R. Martín, K. J. McCarthy, F. Medina, M. Medrano, A. V. Melnikov, P. Mendez, B. van Milligen, I. S. Nedzelskiy, M. Ochando, O. Orozco, J. L. de Pablos, L. Pacios, I. Pastor, M. A. Pedrosa, A. de la Peña, A. Pereira, A. Petrov, S. Petrov, A. Portas, D. Rapisarda, L. Rodríguez-Rodrigo, E. Rodríguez-Solano, J. Romero, A. Salas, E. Sánchez, J. Sánchez, M. Sánchez, K. Sarksian, C. Silva, S. Schchepetov, N. Skvortsova, F. Tabarés, D. Tafalla, A. Tolkachev, V. Tribaldos, I. Vargas, J. Vega, G. Wolfers, and B. Zurro, Nucl. Fusion **45**, S266 (2005).
[5] P. W. Terry, Rev. Mod. Phys. **72**, 109 (2000).
[6] G. D. Conway, Plasma Phys. Controlled Fusion **50**, 124026 (2008).
[7] N. Bretz, Rev. Sci. Instrum. **68**, 2927 (1997).
[8] M. A. Pedrosa, B. A. Carreras, C. Hidalgo, C. Silva, M. Hron, L. García, J. A. Alonso, I. Calvo, J. L. de Pablos, and J. Stöckel, Plasma Phys. Controlled Fusion **49**, B303 (2007).
[9] Ch. P. Ritz, D. L. Brower, T. L. Rhodes, R. D. Bengtson, S. J. Levinson, N. C. Luhmann, W. A. Peebles, and E. J. Powers, Nucl. Fusion **27**, 1125 (1987).
[10] Y. C. Kim and E. J. Powers, Phys. Fluids **21**, 1452 (1978).
[11] Y. C. Kim, J. M. Beall, E. J. Powers, and R. W. Miksad, Phys. Fluids **23**, 258 (1980).
[12] Ch. P. Ritz, E. J. Powers, T. L. Rhodes, R. D. Bengtson, K. W. Gentle, H. Lin, P. E. Phillips, A. J. Wootton, D. L. Brower, N. C. Luhman, Jr., W. A. Peebles, P. M. Schoch, and K. L. Hickok, Rev. Sci. Instrum. **59**, 1739 (1988).
[13] C. Hidalgo, E. Sánchez, T. Estrada, B. Brañas, Ch. P. Ritz, T. Uckan, J. Harris, and A. J. Wootton, Phys. Rev. Lett. **71**, 3127 (1993).
[14] B. Ph. van Milligen, E. Sánchez, T. Estrada, C. Hidalgo, B. Brañas, B. Carreras, and L. García, Phys. Plasmas **2**, 3017 (1995).
[15] B. Ph. van Milligen, C. Hidalgo, and E. Sánchez, Phys. Rev. Lett. **74**, 395 (1995).
[16] H. Y. W. Tsui, K. Rypdal, Ch. P. Ritz, and A. J. Wootton, Phys. Rev. Lett. **70**, 2565 (1993).
[17] Ch. P. Ritz, E. J. Powers, and R. D. Bengtson, Phys. Fluids B **1**, 153 (1989).
[18] A. E. White, S. J. Zweben, M. J. Burin, T. A. Carter, T. S. Hahm, J. A. Krommes, and R. J. Maqueda, Phys. Plasmas **13**, 072301 (2006).
[19] B. Ph. van Milligen, C. Hidalgo, E. Sánchez, M. A. Pedrosa, R. Balbín, I. García-Cortés, and G. R. Tynan, Rev. Sci. Instrum. **68**, 967 (1997).
[20] G. R. Tynan, L. Schmitz, R. W. Conn, R. Doerner, and R. Lehmer, Phys. Rev. Lett. **68**, 3032 (1992).
[21] R. A. Moyer, G. R. Tynan, C. Holland, and M. J. Burin, Phys. Rev. Lett. **87**, 135001 (2001).
[22] P. H. Diamond, M. N. Rosenbluth, E. Sánchez, C. Hidalgo, B. Ph. van Milligen, T. Estrada, B. Brañas, M. Hirsch, H. J. Hartfuss, and B. A. Carreras, Phys. Rev. Lett. **84**, 4842 (2000).
[23] C. P. Perez, H. R. Koslowski, G. T. A. Huysmans, T. C. Hender, P. Smeulders, B. Alper, E. de la Luna, R.J. Hastie, L. Meneses, M. F. F. Nave, V. Parail, M. Zerbini, and JET-EFDA Contributors, Nucl. Fusion **44**, 609 (2004).
[24] F. M. Poli, S. E. Sharapov, S. C. Chapman, and JET-EFDA Contributors, Plasma Phys. Controlled Fusion **50**, 095009 (2008).
[25] C. Riccardi, D. Xuantong, M. Salierno, L. Gamberale, and M. Fontanesi, Phys. Plasmas **4**, 3749 (1997).
[26] F. J. Øynes, O.-M. Olsen, H. L. Pécseli, Å. Fredriksen, and K. Rypdal, Phys. Rev. E **57**, 2242 (1998).
[27] A. A. Ferreira, M. V. A. P. Heller, and I. L. Caldas, Phys. Plasmas **7**, 3567 (2000).
[28] K. Itoh, Y. Nagashima, S.-I. Itoh, P. H. Diamond, A. Fujisawa, M. Yagi, and A. Fukuyama, Phys. Plasmas **12**, 102301 (2005).

[29] Y. Nagashima, K. Hoshino, A. Ejiri, K. Shinohara, Y. Takase, K. Tsuzuki, K. Uehara, H. Kawashima, H. Ogawa, T. Ido, Y. Kusama, and Y. Miura, Phys. Rev. Lett. **95**, 095002 (2005).

[30] H. Lin, Ph.D. thesis, University of Texas, 1991.

[31] M. V. A. P. Heller, R. M. Castro, Z. A. Brasílio, I. L. Caldas, and R. P. Silva, Nucl. Fusion **35**, 59 (1995).

[32] P. Devynck, G. Bonhomme, E. Martines, J. Stöckel, G. Van Oost, I. Voit-sekhovitch, J. Adamek, A. Azeroual, F. Doveil, I. Duran, E. Gravier, J. Gunn, and M. Hron, Plasma Phys. Controlled Fusion **47**, 269 (2005).

[33] M. V. A. P. Heller, I. L. Caldas, A. A. Ferreira, E. A. O. Saettone, A. Vannucci, I. C. Nascimento, and J. H. F. Severo, Czech. J. Phys. **55**, 265 (2005).

[34] M. V. A. P. Heller, I. L. Caldas, A. A. Ferreira, E. A. O. Saettone, and A. Vannucci, J. Plasma Phys. **73**, 295 (2007).

[35] S. E. Sharapov, F. M. Poli, and JET-EFDA Contributors, in *Europhysics Conference Abstracts, 35th EPS Conference on Plasma Physics*, Hersonissos, 2008, edited by P. Lalousis and S. Moustaizis (European Physical Society, Switzerland, 2008), Vol. 32D, p. 4.071.

[36] J. C. Perez, W. Horton, R. D. Bengtson, and T. Carter, Phys. Plasmas **13**, 055701 (2006).

[37] W. Horton, C. Correa, J. Kim, G. D. Chagelishvili, V. S. Avsarkisov, and R. G. Chanishvili, "On generation of Alfvenic-like waves by drift wave zonal flow system in LAPD experiments," Phys. Plasmas (submitted).

[38] S. J. Camargo, M. Tippett, and I. L. Caldas, Phys. Rev. E **58**, 3693 (1998).

[39] F. Militello, F. L. Waelbroeck, R. Fitzpatrick, and W. Horton, Phys. Plasmas **15**, 050701 (2008).

[40] I. C. Nascimento, Yu. K. Kuznetsov, J. H. F. Severo, A. M. M. Fonseca, A. Elfimov, V. Bellintani, M. Machida, M. V. A. P. Heller, R. M. O. Galvão, E. K. Sanada, and J. I. Elizondo, Nucl. Fusion **45**, 796 (2005).

[41] I. C. Nascimento, Yu. K. Kuznetsov, Z. O. Guimarães-Filho, I. El Chamaa-Neto, O. Usuriaga, A. M. M. Fonseca, R. M. O. Galvão, I. L. Caldas, J. H. F. Severo, I. B. Semenov, C. Ribeiro, M. V. A. P. Heller, V. Bellintani, J. I. Elizondo, and E. Sanada, Nucl. Fusion **47**, 1570 (2007).

[42] Z. O. Guimarães-Filho, I. L. Caldas, R. L. Viana, M. V. A. P. Heller, I. C. Nascimento, Yu. K. Kuznetsov, and R. D. Bengtson, Phys. Plasmas **15**, 062501 (2008).

[43] M. S. Baptista, T. P. Silva, J. C. Sartorelli, and I. L. Caldas, Phys. Rev. E **67**, 056212 (2003).

[44] M. S. Baptista, T. Pereira, J. C. Sartorelli, I. L. Caldas, and J. Kurths, Physica D **212**, 216 (2005).

[45] M. S. Baptista, S. P. Garcia, S. K. Dana, and J. Kurths, Eur. Phys. J. Spec. Top. **165**, 119 (2008).

[46] C. M. Ticos, E. Rosa, Jr., W. B. Pardo, J. A. Walkenstein, and M. Monti, Phys. Rev. Lett. **85**, 2929 (2000).

[47] M. S. Davis, N. G. Nutter, and E. Rosa, Jr., Int. J. Bifurcation Chaos Appl. Sci. Eng. **17**, 3513 (2007).

[48] C. Schröder, T. Klinger, D. Block, A. Piel, G. Bonhomme, and V. Naulin, Phys. Rev. Lett. **86**, 5711 (2001).

[49] Z. O. Guimarães-Filho, I. L. Caldas, R. L. Viana, J. Kurths, I. C. Nascimento, and Yu. K. Kuznetsov, Phys. Lett. A **372**, 1088 (2008).

[50] K. Mima and A. Hasegawa, Phys. Rev. Lett. **39**, 205 (1977); Phys. Fluids **21**, 81 (1978).

[51] P. Terry and W. Horton, Phys. Fluids **26**, 106 (1983); **25**, 491 (1982).

[52] C. W. Horton, Rev. Mod. Phys. **71**, 735 (1999).

[53] W. Horton and A. Hasegawa, Chaos **4**, 227 (1994).

[54] R. D. Hazeltine and J. D. Meiss, *Plasma Confinement* (Addison-Wesley, Redwood City, 1992).

[55] A. M. Batista, I. L. Caldas, S. R. Lopes, R. L. Viana, W. Horton, and P. J. Morrison, Phys. Plasmas **13**, 042510 (2006).

[56] A. M. Batista, I. L. Caldas, S. R. Lopes, and R. L. Viana, Philos. Trans. R. Soc. London, Ser. A **366**, 609 (2008).

[57] M. Casdagli, Physica D **108**, 12 (1997).

[58] The literature on recurrence plots is extensive and rapidly growing. A recent review is N. Marwan, M. C. Romano, M. Thiel, and J. Kurths, Phys. Rep. **438**, 237 (2007).

[59] R. M. Castro, M. V. A. P. Heller, I. L. Caldas, R. P. da Silva, Z. A. Brasílio, and I. C. Nascimento, Phys. Plasmas **3**, 971 (1996).

[60] M. V. A. P. Heller, R. M. Castro, I. L. Caldas, Z. A. Brasílio, R. P. Silva, and I. C. Nascimento, J. Phys. Soc. Jpn. **66**, 3453 (1997).

[61] P. Beyer, X. Garbet, and P. Ghendrih, Phys. Plasmas **5**, 4271 (1998).